

Observational signatures of negative mass wormholes through their shadows

Shin'ichi Nojiri^{1,2*}

¹⁾ *KEK Theory Center, Institute of Particle and Nuclear Studies,*

High Energy Accelerator Research Organization (KEK), Oho 1-1, Tsukuba, Ibaraki 305-0801, Japan and

¹⁾ *Kobayashi-Maskawa Institute for the Origin of Particles and the Universe, Nagoya University, Nagoya 464-8602, Japan*

Sergei D. Odintsov^{3,4†}

³⁾ *Institut de Ciències de l'Espai, ICE/CSIC-IEEC, Campus UAB, Carrer de Can Magrans s/n, 08193 Bellaterra (Barcelona), Spain and*

⁴⁾ *Institució Catalana de Recerca i Estudis Avançats (ICREA), Passeig Luis Companys, 23, 08010 Barcelona, Spain*

Diego Sáez-Chillón Gómez^{5,6‡}

⁵⁾ *Department of Theoretical, Atomic and Optical Physics, and Laboratory for Disruptive Interdisciplinary Science (LaDIS), Campus Miguel Delibes, University of Valladolid UVA, Paseo Belén, 7, 47011 Valladolid, Spain and*

⁶⁾ *Department of Physics, Universidade Federal do Ceará (UFC), Campus do Pici, Fortaleza - CE, C.P. 6030, 60455-760 - Brazil*

We investigate systems containing objects with negative mass (NMOs). In a system consisting of one object with positive mass and one NMO, a bound state exists even though the force exerted by the NMO on the object with positive mass is repulsive. Unlike a standard system consisting of two objects with positive mass, the gravitational waves emitted from this system exhibit a decrease in frequency and amplitude over time. We propose a model of the time evolution of the Ellis-Bronnikov wormhole, along with a formulation that eliminates the ghost that appears when constructing the Ellis-Bronnikov wormhole, a candidate for an NMO. Furthermore, numerical simulations are performed to obtain the optical appearance of such NMOs. The observed luminosity is also compared with the Schwarzschild black hole and with the Simpson-Visser wormhole, leading to clear differences in the photon ring substructure around the central object.

I. INTRODUCTION

Although the negative mass object (NMO) is not always consistent with physics, such an object has been studied for a long time. The essay by Luttinger [1] might be the first research article in which the term “negative mass” appeared. After that, the dynamics of the system, which includes NMOs, was studied in detail by Bondi [2], and active research has been done [3–15]. In [16, 17], a wormhole solution is presented, which behaves as a positive mass object in one universe and as an NMO in another universe. The two universes are connected by a wormhole throat. See also [18]. The lensing by NMOs was investigated in [19–24], and the abundance of NMOs was also studied in [25]. Furthermore, zero mass objects were considered in [26–40]. It is also interesting that recently, some observational tests on gravitational waves from NMO binaries were proposed in Ref. [15].

The existence of NMOs is usually considered to be inconsistent. As studied in the mechanics of the elementary course, the Lagrangian of a particle at \mathbf{r} with mass m and the potential $V(\mathbf{r})$ is given by

$$L = \frac{1}{2}m\dot{\mathbf{r}} \cdot \dot{\mathbf{r}} - V(\mathbf{r}) . \quad (1)$$

In the case that the mass m is negative, a ghost appears in the corresponding quantum mechanics and therefore is inconsistent. Recently, the possibility that NMOs might consistently appear in [41], whereas in Ref. [15], possible observational proofs of negative mass binaries are studied. We know the behaviour of a bubble inside water, where the bubble looks as if it has a negative mass because the water around the bubble falls due to gravity. Of course, no ghost appears in the system of the bubble and water. Furthermore, the existence of NMOs might not be so unnatural if we consider the gravity. We should note that the negative cosmological constant is identified with negative energy density. When there is another cosmological fluid besides the negative cosmological constant, we

* nojiri@nagoya-u.jp

† odintsov@ice.csic.es

‡ diego.saez@uva.es

may consider the situation where the total energy density is almost equal to zero. A fluctuation in the fluid may make the density of the fluid smaller in some regions. Then the regions behave as if there are NMOs, like the bubble in the water. Although such fluctuations could not be stable, if we consider the situation where there is a usual positive point mass in the fluid with negative pressure, regions where the energy density is negative may appear. This is because the negative pressure generates the force due to the gradient of the pressure, which balances with the gravity generated by the positive point mass. And as a result, the point mass pushes away the fluid. Such a configuration is stable in general. In [41], the spacetime with an NMO was constructed without ghosts by using two scalar fields.

Moreover, the released images by the Event Horizon Telescope (EHT) of the supermassive black holes at the centre of the M87 and Milky Way galaxies have boosted the research on gravitational physics [42, 43], making it possible to analyse black holes directly from the images. The reconstructed pictures show a central shadow surrounded by a complex structure of light rings, which is the consequence of strong magnetic fields and the emission of the plasma that composes the accretion disk [44] but also due to the high deflection that light experiences near a black hole [27, 45, 46]. Despite every clue indicating that both the central objects in M87 and the Milky Way are actually Kerr black holes, the possibility of observing other non-Kerr objects in the future remains real. Then, motivated by this possibility, a large number of analyses have been conducted to test the Kerr paradigm by simulating the observed luminosity of an accretion disk [47–49]. Such luminosity is highly affected, neglecting accretion disk properties, by the structure of the spacetime, such as the locations of circular orbits for photons, their number and the shape of the potential for null geodesics [50, 51].

In this paper, by starting with the tutorial review of the classical mechanics of the system including NMOs, we find that there exists a bound system composed of one positive mass object and one NMO, in spite that the force which the positive mass object suffers from the NMO is repulsive. This system emitted the gravitational wave, but different from that from the standard system of two positive mass objects, the frequency and the amplitude of the gravitational wave decrease in time. There is a candidate for an NMO, that is, the Ellis-Boronnikov wormhole [16, 17], which was proposed over forty years ago. The wormhole was constructed by using a non-canonical scalar field, which is a ghost. We propose a model which excludes the ghost. We also construct a model where the Ellis-Bronnikov wormhole evolves in time. After reviewing the lensing effect by the NMOs, by using the so-called ray-tracing technique, we show the numerical results for the observed image of NMOs or the Ellis-Bronnikov wormhole.

In the next Section, we review the mechanics of the system, including NMOs, at a tutorial level. Especially, we show that the system of one positive mass object and one NMO can make a bound system, although the positive mass object suffers a repulsive force from the NMO. In Section III, we investigate the gravitational wave emitted from the bound system and find that the frequency and the amplitude of the gravitational wave decrease in time, which is different from the behaviour of the standard gravitational wave emitted from the system of two positive mass objects. The Ellis-Boronnikov wormhole is a candidate for an NMO, but it has been constructed by using a non-canonical scalar field, which is a ghost. In Section IV, we show that the ghost can be eliminated by using a constraint. We like to consider a variation of the Ellis-Bronnikov wormhole, which evolves in time. In order to realise such a solution, we review a non-linear σ model with four scalar fields in Section V. We show that a non-linear σ model whose target space metric is given by the Ricci tensor and ghosts can be eliminated by using constraints. In Section VI, by using the non-linear σ model, we construct a Ellis-Bronnikov-type wormhole and investigate the properties. In Section VII, we review the lensing effect by the NMOs, and we observe that the NMOs play the role of the concave lens as expected. In Section VIII, by using the so-called ray-tracing technique, we investigate the observed image of NMOs or the Ellis-Bronnikov wormhole, numerically. The last section is devoted to the summary and discussion.

II. UNDERGRADUATE MECHANICS OF NEGATIVE MASS OBJECT(S)

We may consider the mechanics on the undergraduate level for the system, including NMOs. Here, as an approximation, we use Newton’s law of mechanics and Newton’s law of gravity. We should note that the kinetic energy of the NMO is unbounded below and therefore when the absolute value of the kinetic energy is large, the particle picture could become invalid.

A. General setup

As in the introductory lecture on mechanics in the undergraduate course, we start with the general setup of the system composed of two particles. The contents in the first part are just iterations in the tutorial textbook of classical mechanics, but in the system including NMO(s), the total mass and the reduced mass can be negative. Then we need to be careful about what could be changed in the system.

We assume that there are two point masses with the position vectors \mathbf{r}_1 and \mathbf{r}_2 and the masses m_1 and m_2 . Then the equations of motion are given by

$$m_1 \ddot{\mathbf{r}}_1 = -\frac{Gm_1 m_2 (\mathbf{r}_1 - \mathbf{r}_2)}{|\mathbf{r}_1 - \mathbf{r}_2|^3}, \quad m_2 \ddot{\mathbf{r}}_2 = \frac{Gm_1 m_2 (\mathbf{r}_1 - \mathbf{r}_2)}{|\mathbf{r}_1 - \mathbf{r}_2|^3}. \quad (2)$$

Then

$$0 = m_1 \ddot{\mathbf{r}}_1 + m_2 \ddot{\mathbf{r}}_2 = \frac{d}{dt} (m_1 \dot{\mathbf{r}}_1 + m_2 \dot{\mathbf{r}}_2), \quad (3)$$

which shows the conservation of the total momentum as usual.

First, we consider the case that $m_1 + m_2 \neq 0$. We will consider the case that $m_1 = m_2$ later, where a strange phenomenon could occur.

We now define the total mass M , the reduced mass μ , the position vector of the center of mass \mathbf{R} and the relative position vector \mathbf{r} , as follows,

$$M \equiv m_1 + m_2, \quad \mu \equiv \frac{m_1 m_2}{m_1 + m_2}, \quad \mathbf{R} \equiv \frac{m_1 \mathbf{r}_1 + m_2 \mathbf{r}_2}{m_1 + m_2}, \quad \mathbf{r} \equiv \mathbf{r}_2 - \mathbf{r}_1. \quad (4)$$

Then we find

$$M \ddot{\mathbf{R}} = 0, \quad \mu \ddot{\mathbf{r}} = -\frac{G\mu M \mathbf{r}}{|\mathbf{r}|^3}. \quad (5)$$

We may also define a total energy E by

$$E \equiv \frac{1}{2} m_1 |\dot{\mathbf{r}}_1|^2 + \frac{1}{2} m_2 |\dot{\mathbf{r}}_2|^2 - \frac{Gm_1 m_2}{|\mathbf{r}_1 - \mathbf{r}_2|} = E_{\text{COM}} + E_{\text{rel}},$$

$$E_{\text{COM}} \equiv \frac{1}{2} M |\dot{\mathbf{R}}|^2, \quad E_{\text{rel}} \equiv \frac{1}{2} \mu |\dot{\mathbf{r}}|^2 - \frac{G\mu M}{|\mathbf{r}|}. \quad (6)$$

Note E , E_{COM} , E_{rel} are conserved, respectively.

The second equation of Eq. (5) tells that the motion of the particle(s) is generated by the central force with respect to the relative position vector \mathbf{r} . Therefore the angular momentum \mathbf{L} with respect to the relative position vector \mathbf{r} ,

$$\mathbf{L} = \mu \mathbf{r} \times \dot{\mathbf{r}}, \quad (7)$$

is conserved. Then the motion is restricted to a plane perpendicular to \mathbf{L} , and the plane includes the origin of \mathbf{r} . We choose the plane as the xy -plane, and we use the following polar coordinates,

$$x = r \cos \theta, \quad y = r \sin \theta. \quad (8)$$

Then we find

$$\mathbf{L} = (0, 0, l) = (0, 0, \mu r^2 \dot{\theta}). \quad (9)$$

Here l is a constant corresponding to the absolute value of the angular momentum \mathbf{L} , which is conserved. For a while, we assume $l > 0$.

The last expression in Eq. (6) has the following form,

$$E_{\text{rel}} = \frac{1}{2} \mu (\dot{r}^2 + r^2 \dot{\theta}^2) - \frac{G\mu M}{r}. \quad (10)$$

Further by using (9), we may delete $\dot{\theta}$ in (10),

$$E_{\text{rel}} = \frac{1}{2} \mu \dot{r}^2 + U(r), \quad U(r) \equiv \frac{l^2}{2\mu r^2} - \frac{G\mu M}{r} = \frac{l^2}{2\mu} \left(\frac{1}{r} - \frac{G\mu^2 M}{l^2} \right)^2 - \frac{G^2 \mu^3 M^2}{2l^2}. \quad (11)$$

The expression is an analogue of the particle which moves on a one-dimensional line with a potential $U(r)$. We further rewrite (11) as follows,

$$\frac{2E_{\text{rel}}}{\mu} - \frac{l^2}{\mu^2} \left(\frac{1}{r} - \frac{G\mu^2 M}{l^2} \right)^2 + \frac{G^2 \mu^2 M^2}{l^2}$$

$$= \frac{l^2}{\mu^2} \left(\frac{1}{r} - \frac{G\mu^2 M}{l^2} - \sqrt{\frac{\mu^2}{l^2} \left(\frac{G^2 \mu^2 M^2}{l^2} + \frac{2E_{\text{rel}}}{\mu} \right)} \right) \left(\frac{1}{r} - \frac{G\mu^2 M}{l^2} + \sqrt{\frac{\mu^2}{l^2} \left(\frac{G^2 \mu^2 M^2}{l^2} + \frac{2E_{\text{rel}}}{\mu} \right)} \right) = \dot{r}^2 \geq 0. \quad (12)$$

Eq. (12) tells

$$\frac{2E_{\text{rel}}}{\mu} + \frac{G^2 \mu^2 M^2}{l^2} \geq 0. \quad (13)$$

When $\frac{2E_{\text{rel}}}{\mu} = -\frac{G^2 \mu^2 M^2}{l^2} < 0$, the orbit becomes a circle with a radius,

$$r = \frac{l^2}{G\mu^2 M}. \quad (14)$$

When $\frac{2E_{\text{rel}}}{\mu} > 0$, the orbit is restricted to

$$\frac{1}{r} > \frac{G\mu^2 M}{l^2} + \sqrt{\frac{\mu^2}{l^2} \left(\frac{G^2 \mu^2 M^2}{l^2} + \frac{2E_{\text{rel}}}{\mu} \right)}, \quad (15)$$

which corresponds to a hyperbolic trajectory. When $\frac{2E_{\text{rel}}}{\mu} = 0$, the orbit is a parabolic trajectory. When $0 > \frac{2E_{\text{rel}}}{\mu} > -\frac{G^2 \mu^2 M^2}{l^2}$, the orbit is restricted to

$$\frac{G\mu^2 M}{l^2} + \sqrt{\frac{\mu^2}{l^2} \left(\frac{G^2 \mu^2 M^2}{l^2} + \frac{2E_{\text{rel}}}{\mu} \right)} > \frac{1}{r} > \frac{G\mu^2 M}{l^2} - \sqrt{\frac{\mu^2}{l^2} \left(\frac{G^2 \mu^2 M^2}{l^2} + \frac{2E_{\text{rel}}}{\mu} \right)}, \quad (16)$$

which corresponds to an elliptical trajectory.

The shape of the orbit can be find by rewriting Eq. (11) by using (9) as follows,

$$E_{\text{rel}} = \frac{l^2}{2\mu r^4} \left(\frac{dr}{d\theta} \right)^2 + U(r). \quad (17)$$

By solving (17) with respect to $r = r(\theta)$, we obtain

$$r = \frac{\frac{l^2}{G\mu^2 M}}{1 + \cos(\theta - \theta_0) \sqrt{1 + \frac{2l^2 E_{\text{rel}}}{G^2 \mu^3 M^2}}}. \quad (18)$$

Here θ_0 is a constant of the integration. Therefore when $\frac{E_{\text{rel}}}{\mu} > 0$, the orbit becomes a hyperbola, when $\frac{E_{\text{rel}}}{\mu} = 0$, the orbit becomes a parabola, when $0 > \frac{E_{\text{rel}}}{\mu} > -\frac{G^2 \mu^2 M^2}{2l^2}$, the orbit becomes an ellipse and when $\frac{E_{\text{rel}}}{\mu} = -\frac{G^2 \mu^2 M^2}{2l^2} < 0$, the orbit becomes a circle.

We may consider the case $l = 0$, where (10) has the following form,

$$E_{\text{rel}} = \frac{1}{2} \mu \dot{r}^2 - \frac{G\mu M}{r}. \quad (19)$$

This requires

$$\frac{E_{\text{rel}}}{\mu} + \frac{GM}{r} \geq 0. \quad (20)$$

When $l = 0$, the two objects move on the straight line connecting them and the objects might collide with each other.

When $\frac{E_{\text{rel}}}{\mu M} > 0$, Eq. (20) tells $M > 0$. Then we solve (19) as follows,

$$t - t_0 = \mp \sqrt{\frac{\mu}{2E_{\text{rel}}}} \frac{G\mu M}{2E_{\text{rel}}} \left\{ -2\sqrt{1 + \frac{G\mu M}{E_{\text{rel}} r}} + \ln \frac{\sqrt{1 + \frac{G\mu M}{E_{\text{rel}} r}} + 1}{\sqrt{1 + \frac{G\mu M}{E_{\text{rel}} r}} - 1} \right\}, \quad (21)$$

Here, t_0 is a constant of the integration. When $r \rightarrow 0$, we obtain

$$t - t_0 \rightarrow 0. \quad (22)$$

Then two objects with m_1 and m_2 might collide with each other in a finite time, but the two objects might move in opposite directions.

When $\frac{E_{\text{rel}}}{\mu M} < 0$, there are the case that M is positive and the case that M is negative. In the case of $M > 0$, we obtain,

$$t - t_0 = \mp \sqrt{-\frac{\mu}{2E_{\text{rel}}}} \frac{G\mu M}{2E_{\text{rel}}} \left\{ \frac{2\sqrt{-1 - \frac{G\mu M}{E_{\text{rel}}r}}}{\frac{G\mu M}{E_{\text{rel}}r}} + 2 \arctan \frac{1}{\sqrt{-1 - \frac{G\mu M}{E_{\text{rel}}r}}} \right\}, \quad (23)$$

When $r \rightarrow 0$, we obtain

$$t - t_0 \rightarrow 0. \quad (24)$$

Then two objects with m_1 and m_2 can collide with each other in a finite time, again. We also note that Eq. (20) tells that r has an upper limit,

$$r \leq r_{\text{max}} \equiv -\frac{G\mu M}{E_{\text{rel}}}. \quad (25)$$

Therefore, the system is bound, but the two objects must collide with each other.

On the other hand when $\frac{E_{\text{rel}}}{\mu M} < 0$ and $M < 0$, we obtain,

$$t - t_0 = \mp \sqrt{-\frac{\mu}{2E_{\text{rel}}}} \frac{G\mu M}{2E_{\text{rel}}} \left\{ -\frac{2\sqrt{1 + \frac{G\mu M}{E_{\text{rel}}r}}}{\frac{G\mu M}{E_{\text{rel}}r}} + \ln \frac{\sqrt{1 + \frac{G\mu M}{E_{\text{rel}}r}} + 1}{\sqrt{1 + \frac{G\mu M}{E_{\text{rel}}r}} - 1} \right\}, \quad (26)$$

Eq. (19) tells that r has a minimum

$$r \geq r_{\text{min}} \equiv -\frac{G\mu M}{E_{\text{rel}}}. \quad (27)$$

Then two objects with m_1 and m_2 cannot collide with each other. That is, the two objects with m_1 and m_2 do not make a bound system.

For completeness, we may consider the case of $E_{\text{rel}} = 0$ in (19). For consistency, we find $M \geq 0$. Because r is a constant when $M = 0$, we may further assume $M > 0$. Then the solution of (19) is given by

$$r^{\frac{3}{2}} = \frac{3}{2} \sqrt{2GM} (t - t_0). \quad (28)$$

Here, t_0 is a constant of the integration, again. We obtain $r = 0$ when $t = t_0$, and therefore the two objects might collide with each other in a finite time.

B. $m_1, m_2 > 0$ case

First, we consider the case that both m_1 and m_2 are positive, as written in any introductory textbook. In this case, M and μ are also positive. Therefore if $l > 0$, when $E_{\text{rel}} > 0$, the orbit becomes a hyperbola, when $E_{\text{rel}} = 0$, the orbit becomes a parabola, when $0 > E_{\text{rel}} > -\frac{G^2\mu^3M^2}{2l^2}$, the orbit becomes an ellipse and when $E_{\text{rel}} = -\frac{G^2\mu^3M^2}{2l^2} < 0$, the orbit becomes a circle.

Even if $l = 0$, $E_{\text{rel}} \geq 0$, the system is not bound although when $E_{\text{rel}} < 0$, it is bound as in (25). In the case of $l = 0$, the two objects might collide with each other.

C. $m_1, m_2 < 0$ case

When both of m_1 and m_2 are negative, M and μ are also negative. Eq. (10) tells that $\frac{E_{\text{rel}}}{\mu}$ is always positive. Therefore, the only possible orbit when $l > 0$ is a hyperbola, and any bound state does not appear.

Because $\frac{E_{\text{rel}}}{\mu M} < 0$, when $l = 0$, the solution is given by (26). There is a minimum for r as in (27).

D. $m_1 > 0, m_2 < 0$ and $m_1 + m_2 \neq 0$ case

When $m_1 > 0, m_2 < 0$ and $m_1 + m_2 \neq 0, \mu$ and M can be positive or negative.

First, we consider the case $l > 0$. Eq. (10) tells that if M is negative, $\frac{E_{\text{rel}}}{\mu}$ is positive and therefore only possible orbit is a hyperbola. On the other hand, if M is positive, $\frac{E_{\text{rel}}}{\mu}$ can be negative or positive. Therefore when $\frac{E_{\text{rel}}}{\mu} > 0$, the orbit becomes a hyperbola, when $\frac{E_{\text{rel}}}{\mu} = 0$, the orbit becomes a parabola, when $0 > \frac{E_{\text{rel}}}{\mu} > -\frac{G^2 \mu^2 M^2}{2l^2}$, the orbit becomes an ellipse and when $\frac{E_{\text{rel}}}{\mu} = -\frac{G^2 \mu^2 M^2}{2l^2} < 0$, the orbit becomes a circle.

We should note that when $m_1 > -m_2$, the position vector of the centre of mass \mathbf{R} lies on the straight line connecting the point mass with $m_1 > 0$ and the point mass with $m_2 < 0$ and outside of the point mass with $m_1 > 0$ as shown in FIG. 1. In fact, if we choose $\mathbf{r}_1 = (0, 0, 0)$ and $\mathbf{r}_2 = (0, r, 0)$ with $r > 0$, we find $\mathbf{R} = \left(0, \frac{m_2 r}{m_1 + m_2}, 0\right)$. We should note $\frac{m_2 r}{m_1 + m_2}$ is negative, $\frac{m_2 r}{m_1 + m_2} < 0$. The point mass with m_1 suffers a repulsive force from the point mass with m_2 , and the force becomes a centripetal force for the point mass with m_1 to the centre of mass. Therefore, when $m_1 > -m_2$ and $\frac{E_{\text{rel}}}{\mu} < 0$, two point masses with mass $m_1 > 0$ and $m_2 < 0$ make a bound state.

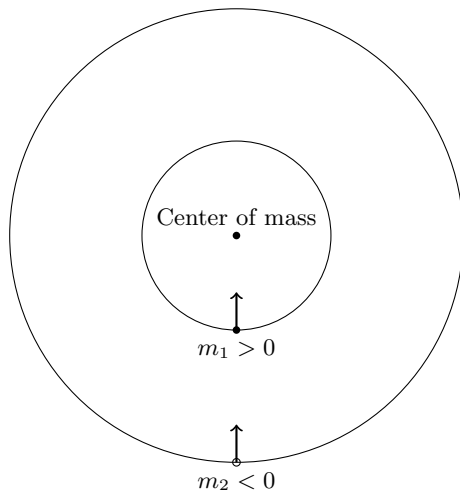


FIG. 1. When $m_1 > -m_2$, the position vector of the centre of mass \mathbf{R} lies on the straight line connecting the point mass with $m_1 > 0$ and the point mass with $m_2 < 0$ and outside of the point mass with $m_1 > 0$. The point mass with m_1 suffers a repulsive force from the point mass with m_2 , and the force becomes a centripetal force for the point mass with m_1 to the centre of mass. Therefore, when $m_1 > -m_2$ and $\frac{E_{\text{rel}}}{\mu} < 0$, two point masses with mass $m_1 > 0$ and $m_2 < 0$ make a bound state.

We may also consider the $l = 0$ case. Eq. (4) tells that if M is positive, μ is negative, and if M is negative, μ is positive. Therefore if $E_{\text{rel}} > 0, \frac{E_{\text{rel}}}{\mu M} < 0$, and if $E_{\text{rel}} < 0, \frac{E_{\text{rel}}}{\mu M} > 0$. This tells that in the case that $E_{\text{rel}} > 0$ and $M > 0$, the solution is given by (23), which is a bound system. In the case that $E_{\text{rel}} > 0$ and $M < 0$, the solution is given by (26), where the system is not bound. In the case that $E_{\text{rel}} < 0$ and $M > 0$, the solution is given by (21), which is not a bound system. The case that $E_{\text{rel}} < 0$ and $M < 0$ is kinematically forbidden. In the case

E. $m_1 = -m_2 = m > 0$ case

We may also consider a special case $m_1 = -m_2 = m > 0$, where the total mass M in (4) vanishes and the reduced mass μ and the position vector of the centre of mass \mathbf{R} diverge.

Eq. (3) reduces

$$\dot{\mathbf{r}}_1 - \dot{\mathbf{r}}_2 = \mathbf{v}_0, \quad \mathbf{r}_1 - \mathbf{r}_2 = \mathbf{v}_0 (t - t_0). \quad (29)$$

Here \mathbf{v}_0 is a constant vector and in the second equation in (29), t_0 is a constant of the integration. Then the equations in (2) have the following form

$$m\ddot{\mathbf{r}}_1 = -m\ddot{\mathbf{r}}_2 = -\frac{Gm^2\mathbf{v}_0}{|\mathbf{v}_0|^3 (t - t_0)^2}, \quad (30)$$

whose solution is

$$\mathbf{r}_1 = \mathbf{r}_2 + \mathbf{v}_0 (t - t_0) = \frac{Gm^2 \mathbf{v}_0}{|\mathbf{v}_0|^3} \ln \frac{t - t_0}{t_0} + \mathbf{v}_1 t + \mathbf{r}_0. \quad (31)$$

Here \mathbf{v}_1 and \mathbf{r}_0 are vectors for the constants of the integration. If there are two objects before t_0 , $t < t_0$, the second equation of Eq. (29) tells that the two objects collide with each other and they may vanish. The singular behaviour as $t \rightarrow t_0$ could indicate that Newton's approximations for gravity and mechanics become invalid. In [52], the above behaviours have been considered. This is so-called runaway motion [2].

The above calculations are, of course, not intended as a fundamental model of negative-mass particles. As we mentioned in the introduction, in elementary mechanics, a negative inertial mass gives a kinetic energy unbounded from below, so such a point particle cannot be a stable microscopic degree of freedom. In this section, the signed mass is used only as an effective weak-field parameter, or it may represent the leading gravitational response of a hypothetical extended or geometrical object that behaves, at large distances, as if it had negative mass, as discussed in [41]. Within that approximation, the Newtonian two-body problem shows that positive/negative-mass systems can admit bounded relative orbits, which then provide the basis for the gravitational-wave discussion in Section III.

III. GRAVITATIONAL WAVE

The bound system of two objects generates a gravitational wave due to its rotation. We now investigate the difference between the system of two positive mass objects and the system of one positive mass object and one NMO. For the system of one positive mass object and one NMO, we assume the total mass $M = m_1 + m_2$ is positive, but the reduced mass $\mu = \frac{m_1 m_2}{m_1 + m_2}$ is negative.

For simplicity, we consider the circle orbit in (14). By using (9), we find

$$\dot{\theta} = \frac{l}{\mu r^2} = \frac{G^2 \mu^3 M^2}{l^3}. \quad (32)$$

Then the frequency f of the rotation is given by

$$f = \frac{|\dot{\theta}|}{2\pi} = \frac{G^2 |\mu|^3 M^2}{2\pi l^3} = \frac{\sqrt{GM}}{2\pi r^{\frac{3}{2}}}. \quad (33)$$

Here we used (14). We also defined f to be positive. The relation between the frequency f and the radius r is nothing but Kepler's third law. Therefore, the expression (33) is valid for both the system of two positive mass objects and the system of one positive mass object and one NMO.

The gravitational wave h emitted has the following form,

$$h \sim \frac{4G\mu}{D} (2\pi r f)^2 \sin(4\pi f t) = \frac{4G^2 M \mu}{D r} \sin\left(\frac{2\sqrt{GM}}{r^{\frac{3}{2}}} t\right). \quad (34)$$

Here D is the distance from the observer.

The rotation generates the oscillation of the quadratic moment, which induces the gravitational wave. Eq. (33) also gives the frequency of the gravitational wave. The emitted energy induces a decrease in the energy E of the system, and it can be expressed as

$$\frac{dE}{dt} = -\frac{32G^4 \mu^2 M^3}{5r^5}, \quad (35)$$

which is, of course, negative even for the system of one positive mass object and one NMO. The formula (35) was originally derived within the post-Newtonian general relativity for systems with positive mass and standard stress-energy. The gravitational wave (34), however, always carries positive energy and therefore dE/dt is always negative. The emission of the gravitational wave is generated by the oscillation of the quadratic moment, and therefore, if we know the frequency and the magnitude of the quadratic moment, we can estimate the emitted energy. Therefore, the formula (35) can be applied even for the system including NMO(s).

Because the radius of the circle is given by (14), the energy E_{rel} is expressed as

$$E_{\text{rel}} = -\frac{G\mu M}{2r}. \quad (36)$$

Now we identify E in (35) with E_{rel} . We should note that the energy E_{rel} must decrease by the emission of the gravitational wave. For the system of the two positive mass objects, due to the emission of the gravitational wave, the radius r becomes shorter because the energy E_{rel} must decrease. Then the frequency f (33) becomes larger and larger. On the other hand, in the system with one positive mass and one NMO, because E_{rel} in (36) is positive, r becomes larger by the emission and therefore the frequency f in (33) becomes smaller. By the emission of the gravitational wave, the positive mass object and the NMO do not merge. Therefore, we can distinguish the system of two positive mass objects and the system with one positive mass and one NMO.

By identifying $E = E_{\text{rel}}$ and combining (35) and (36), we obtain

$$\frac{G\mu M\dot{r}}{2r^2} = -\frac{32G^4\mu^2M^3}{5r^5}, \quad (37)$$

which can be integrated to be

$$r^4 = \frac{2^8}{5}G^3\mu M^2(t_0 - t). \quad (38)$$

Here, t_0 is a constant of the integration. Then the frequency (33) of the emitted gravitational wave has the following time dependence

$$f = \frac{\sqrt{GM}}{2^4\pi} \left\{ \frac{G^3\mu M^2}{5}(t_0 - t) \right\}^{-\frac{3}{8}}. \quad (39)$$

Then the gravitational wave h in (34) is given by

$$h \sim \frac{5^{\frac{1}{4}}G^{\frac{5}{4}}M^{\frac{1}{2}}\mu}{D\left\{\mu(t_0 - t)^{\frac{1}{4}}\right\}} \sin\left(\frac{\sqrt{GM}}{2^2} \left\{ \frac{G^3\mu M^2}{5}(t_0 - t) \right\}^{-\frac{3}{8}} t\right). \quad (40)$$

Both the amplitude and the frequency diverge as $t \rightarrow t_0$, although the Newton approximations will be invalid there. In the gravitational wave for the system with two positive mass objects, the frequency and the amplitude rapidly increase when $t \rightarrow t_0$. On the other hand, in the behaviour of the gravitational wave for the system with one positive mass object and an NMO, the frequency and the amplitude decrease when t increases. We should note $t > t_0$ because $\mu < 0$ for the system with one positive mass object and an NMO. This tells us that if we find the gravitational wave where the frequency and the amplitude decrease, this might be the gravitational wave emitted from the system of one positive mass object and an NMO.

On the other hand, the emitted energy per time in (35) has the following form,

$$\frac{dE}{dt} = -\frac{32G^4\mu^2M^3}{5 \cdot 2^{10}} \left\{ \frac{G^3\mu M^2}{5}(t_0 - t) \right\}^{-\frac{5}{4}}, \quad (41)$$

which gives the amplitude of the emitted gravitational wave.

In the case of the two positive mass objects, where, of course, $\mu > 0$, Eq. (38) tells that $t < t_0$, but when $t \rightarrow t_0$, the two objects collide with each other and may merge. When $t \sim t_0$, Newton's law of gravity must be replaced with Einstein's general relativity, and the internal structure of the objects also becomes important. Eq. (39) tells that the frequency becomes very large when $t \rightarrow t_0$ and the emitted energy expressed by Eq. (41) also diverges.

On the other hand, in a system where one object has a positive mass and another object has a negative mass, although the total mass is positive, Eq. (38) tells that $t > t_0$. because $\mu < 0$. Eq. (38) also tells that the distance between two objects becomes larger and larger. Eqs. (39) and (41) tell that both the frequency and the emitted energy become smaller and smaller in time. The behaviours are very different from those of the system with two positive mass objects. Therefore, if we observe the gravitational wave where the frequency and the intensity decrease, this might be the gravitational wave emitted from the system of one positive mass object and an NMO.

The propagating speed of the gravitational wave could be identical to that of light. Although it depends on how the NMOs are generated, as in [41], if the scalar fields could construct the NMOs, the backreaction of the scalar fields may affect the propagation as observed in [53].

IV. GHOST-FREE ELLIS-BRONNIKOV WORMHOLE

A candidate of the NMO is a wormhole solution found in [16, 17]. In one universe, the wormhole behaves as a positive mass object; in another universe connected to the first by the throat, the wormhole behaves as an NMO.

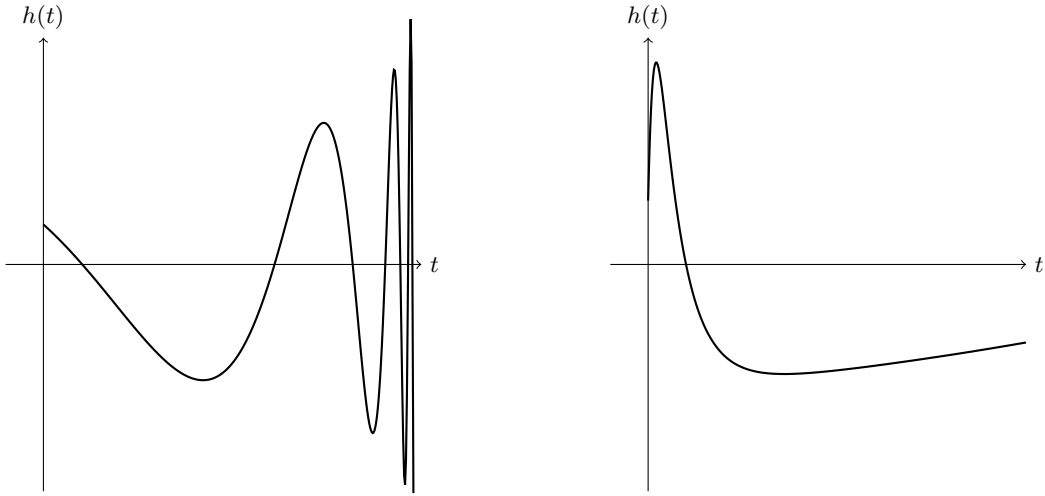


FIG. 2. The left figure shows the behaviour of the gravitational wave for the system with two positive mass objects. The frequency and the amplitude rapidly increase when $t \rightarrow t_0$. The right figure shows the behaviour of the gravitational wave for the system with one positive mass object and an NMO. The frequency and the amplitude decrease when t increases. If we observe the gravitational wave where the frequency and the amplitude decrease, this might be the gravitational wave emitted from the system of one positive mass object and an NMO.

The wormhole is realised by Einstein's gravity coupled with a scalar field ϕ with a non-canonical kinetic term, whose action is given by,

$$S = \frac{1}{2\kappa^2} \int d^4x \sqrt{-g} (R + 2g^{\mu\nu} \partial_\mu \phi \partial_\nu \phi). \quad (42)$$

The wormhole solution is given by [18]

$$\begin{aligned} ds^2 &= -e^{2\nu(r)} dt^2 + e^{-2\nu(r)} dr^2 + (r^2 + q^2 - M^2) e^{-2\nu(r)} (d\vartheta^2 + \sin^2 \vartheta d\varphi^2), \\ \phi(r) &= -\frac{q\nu(r)}{M}, \\ \nu(r) &= -\frac{2M}{\sqrt{q^2 - M^2}} \arctan\left(\frac{r}{\sqrt{q^2 - M^2}}\right), \end{aligned} \quad (43)$$

Here, q appears as a constant of the integration and the coordinate r ranges from $-\infty$ to $+\infty$, where positive r may correspond to our universe and negative r to another universe. Because $\arctan x = \frac{\pi}{2} - x^{-1} + \frac{x^{-3}}{3} + \mathcal{O}(x^{-5})$ when $x \rightarrow +\infty$ and $\arctan x = -\frac{\pi}{2} + x^{-1} + \frac{x^{-3}}{3} + \mathcal{O}(x^{-5})$ when $x \rightarrow -\infty$, when $|r|$ is large, in our universe ($r > 0$), $e^{2\nu(r)}$ behaves as

$$e^{2\nu(r)} \sim e^{-\frac{2\pi}{\sqrt{q^2 - M^2}}} \left(1 - \frac{4M}{r} + \mathcal{O}(r^{-2})\right), \quad (44)$$

and in another universe ($r < 0$), we find

$$e^{2\nu(r)} \sim e^{\frac{2\pi}{\sqrt{q^2 - M^2}}} \left(1 + \frac{4M}{r} + \mathcal{O}(r^{-2})\right), \quad (45)$$

The factor $e^{\mp \frac{2\pi}{\sqrt{q^2 - M^2}}}$ could be absorbed into the redefinition of the time coordinate t . Then Eq. (44) tells that the wormhole behaves as a positive mass object in our universe, and Eq. (45) tells that the wormhole behaves as an NMO. Then the usual matter with positive mass may fall into the wormhole in our universe, but due to the negative mass of the wormhole in another universe, the fallen matter is blown out by the repulsive force into another universe, as in the white hole. Therefore, the Ellis-Bronnikov wormhole plays the role of a pump of matter from another universe to our universe, as shown in FIG. 3. For the electromagnetic wave or gravitational wave, if the wave emitted in the

universe where the wormhole looks to have a negative mass goes through the wormhole throat, the wave appearing in the universe where the wormhole looks to have a positive mass will be redshifted. On the contrary, the wave emitted in the universe with the wormhole with positively looking mass will be blueshifted if the wave appears in the universe with the wormhole with negatively looking mass.

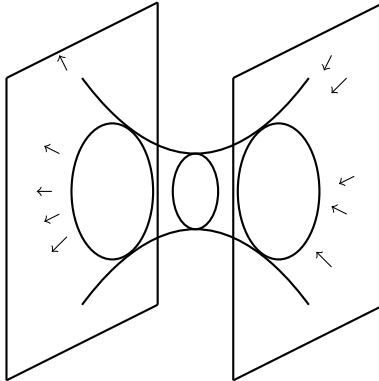


FIG. 3. An object sucked into a wormhole that behaves as if it has positive mass is ejected from a wormhole that behaves as if it has negative mass.

Because the scalar field ϕ in (42) is a ghost, the model is physically inconsistent. In order to remove the ghost, we use the formulation as in [54–58]. First, we define a new scalar field χ by

$$\phi = \phi(r = \chi), \quad (46)$$

that is, in the solution (43), $\chi = r$. For χ , we add the following action with a Lagrange multiplier field λ to the action (42),

$$S_\lambda = \int d^4x \sqrt{-g} \lambda \left(e^{2\nu(r=\chi)} g^{\mu\nu} \partial_\mu \chi \partial_\nu \chi - 1 \right). \quad (47)$$

By the variation of the action S_χ with respect to λ , we obtain the following constraint,

$$0 = e^{2\nu(r=\chi)} g^{\mu\nu} \partial_\mu \chi \partial_\nu \chi - 1, \quad (48)$$

which is consistent with the solution (43), $\chi = r$. The constraint (48) eliminates the ghost and there is always a solution $\lambda = 0$ with (43) [54–58].

V. SPACETIME AND TARGET-SPACE GEOMETRIES IN NON-LINEAR σ MODEL WITH FOUR SCALAR FIELDS

We now try to construct a spacetime where an Ellis-Bronnikov-type wormhole is created, as in the wormhole creation in [55, 57, 59]. For this purpose, we use the formulation proposed in [60, 61]. In the formulation, an arbitrary geometry can be realised using a non-linear σ model whose target-space metric is identified with the Ricci curvature. Therefore, the non-linear σ model has four scalar components in four dimensions, and the four scalar fields correspond to the spacetime coordinates. Note that in d dimensions, the minimal number of scalar fields is d .

The action of the non-linear σ model including four scalar components ϕ^a ($a = 0, 1, 2, 3$) coupled to Einstein gravity is given by,

$$S = S_{\text{gravity}} + S_\phi + S_\lambda, \quad (49)$$

$$S_{\text{gravity}} = \frac{1}{2\kappa^2} \int d^4x \sqrt{-g} R, \quad (50)$$

$$S_\phi \equiv \frac{1}{2} \int d^4x \sqrt{-g} \sum_{a,b=0,1,2,3} A_{ab}(\phi) g^{\mu\nu} \partial_\mu \phi^a \partial_\nu \phi^b, \quad (51)$$

$$S_\lambda \equiv \int d^4x \sqrt{-g} \sum_{a=0,1,2,3} \lambda^a \left(\frac{1}{g^{aa}(x=\phi)} g^{\mu\nu}(x) \partial_\mu \phi^a \partial_\nu \phi^a - 1 \right). \quad (52)$$

Here, the Roman indices ($a, b, \dots = 0, 1, 2, 3$) are used for the scalar fields, corresponding to indices in the internal space. The kinetic coefficient functions $A_{ab}(\phi)$ are functions of the scalar fields ϕ^a . In Eq. (52), we introduce λ^a 's as Lagrange multiplier fields, which impose the following constraints,

$$0 = \frac{1}{g^{aa}(x=\phi)} g^{\mu\nu}(x) \partial_\mu \phi^a \partial_\nu \phi^a - 1. \quad (53)$$

The constraints in Eq. (53) make the model to be ghost-free [60, 61]. These constraints (53) also prohibit the propagation of the scalar fields. Although the scalar fields generate energy density and pressure as in the standard fluid, sound propagation does not appear and therefore, even if any energy condition is violated, the scalar fields do not generate any instability.

The variation of the action (49) with respect to the metric $g_{\mu\nu}$ gives

$$\begin{aligned} \mathcal{G}_{\mu\nu} &= \frac{1}{4} g_{\mu\nu} \sum_{a,b=0,1,2,3} A_{ab}(\phi) - \frac{1}{2} \sum_{a,b=0,1,2,3} A_{ab}(\phi) \partial_\mu \phi^a \partial_\nu \phi^b \\ &\quad + \frac{1}{2} g_{\mu\nu} \sum_{a=0,1,2,3} \lambda^a \left(\frac{1}{g^{aa}(x=\phi)} g^{\mu\nu}(x) \partial_\mu \phi^a \partial_\nu \phi^a - 1 \right) - \sum_{a=0,1,2,3} \frac{\lambda^a}{g^{aa}(x=\phi)} \partial_\mu \phi^a \partial_\nu \phi^a \\ &= \frac{1}{4} g_{\mu\nu} \sum_{a,b=0,1,2,3} A_{ab}(\phi) g^{\xi\eta} \partial_\xi \phi^a \partial_\eta \phi^b - \frac{1}{2} \sum_{a,b=0,1,2,3} A_{ab}(\phi) \partial_\mu \phi^a \partial_\nu \phi^b - \sum_{a=0,1,2,3} \frac{\lambda^a}{g^{aa}(x=\phi)} \partial_\mu \phi^a \partial_\nu \phi^a. \end{aligned} \quad (54)$$

The constraint equations Eq. (53) are used here and $\mathcal{G}_{\mu\nu}$ is defined by using the Einstein tensor $G_{\mu\nu}$ as follows,

$$\mathcal{G}_{\mu\nu} = -\frac{1}{2\kappa^2} G_{\mu\nu} = -\frac{1}{2\kappa^2} \left(R_{\mu\nu} - \frac{1}{2} g_{\mu\nu} R \right). \quad (55)$$

By contracting Eq. (54) with the metric $g^{\mu\nu}$, we find

$$g^{\mu\nu} \mathcal{G}_{\mu\nu} = \frac{1}{2} \sum_{a,b=0,1,2,3} A_{ab}(\phi) g^{\xi\eta} \partial_\xi \phi^a \partial_\eta \phi^b - \sum_{a=0,1,2,3} \lambda^a. \quad (56)$$

Here we used Eq. (53), again. By substituting Eq. (56) into Eq. (54), we obtain

$$\sum_{a,b=0,1,2,3} A_{ab}(\phi) \partial_\mu \phi^a \partial_\nu \phi^b = -2\mathcal{G}_{\mu\nu} + g_{\mu\nu} \left\{ \sum_{a=0,1,2,3} \lambda^a + g^{\rho\sigma} \mathcal{G}_{\rho\sigma} \right\} - 2 \sum_{a=0,1,2,3} \frac{\lambda^a}{g^{aa}(x=\phi)} \partial_\mu \phi^a \partial_\nu \phi^a. \quad (57)$$

We may identify the four scalar fields with the spacetime coordinates $\phi^a = x^a$. This is consistent with the constraints in Eq. (53). This allows us to rewrite Eq. (57),

$$A_{\mu\nu}(\phi) = -2\mathcal{G}_{\mu\nu} + g_{\mu\nu} \left\{ \sum_{a=0,1,2,3} \lambda^a + g^{\rho\sigma} \mathcal{G}_{\rho\sigma} \right\} - 2 \sum_{a=0,1,2,3} \frac{\lambda^a}{g^{aa}(x=\phi)} \delta_\mu^a \delta_\nu^a. \quad (58)$$

We should note that we can consider the solution $\lambda^a = 0$. Therefore an arbitrary geometry specified by the metric $g_{\mu\nu}$ can be realised by choosing the kinetic coefficients $A_{\mu\nu}(\phi)$ as follows,

$$A_{\mu\nu}(\phi) = -2\mathcal{G}_{\mu\nu}(x=\phi) + g_{\mu\nu}(x=\phi) g^{\rho\sigma}(x=\phi) \mathcal{G}_{\rho\sigma}(x=\phi). \quad (59)$$

This tells that the action S_ϕ (49) is that of a non-linear σ model whose target-space metric is given by $A_{ab}(\phi)$.

For Einstein gravity, Eq. (59) is explicitly write as,

$$A_{\mu\nu}(\phi) = \frac{1}{\kappa^2} G_{\mu\nu}(x=\phi) - \frac{1}{2\kappa^2} g_{\mu\nu}(x=\phi) g^{\rho\sigma}(x=\phi) G_{\rho\sigma}(x=\phi) = \frac{1}{\kappa^2} R_{\mu\nu}(x=\phi). \quad (60)$$

It might be interesting that $A_{\mu\nu}(\phi)$ is given by the Ricci tensor $R_{\mu\nu}$. Here the coordinate-dependence of the Ricci tensor $R_{\mu\nu}$ are replaced by the scalar fields-dependence, $x^\mu = \phi^\mu$. Hence, we have shown that any geometry can be realised by a non-linear σ model whose target space metric is given by the Ricci curvature.

VI. DYNAMICAL WORMHOLE: CREATION OF ELLIS-BRONNIKOV-TYPE WORMHOLE

As in [55, 57, 59], we consider the dynamical Ellis-Bronnikov-type wormhole geometry. A general class of the dynamical wormhole could be described by the following metric,

$$ds^2 = e^{2\nu(r,t)} dt^2 + e^{2\lambda(r,t)} dr^2 + (r^2 + a(t)) (d\vartheta^2 + \sin^2 \vartheta d\varphi^2), \quad (61)$$

Here r runs from $-\infty$ to $+\infty$. When $a(t) > 0$, $\sqrt{a(t)}$ corresponds to the radius of the wormhole throat. The throat connects the two universes corresponding to positive r and negative r . We may consider the model,

$$\nu = -\lambda = -\frac{2M}{\sqrt{r^2 + r_0^2}} \tanh \frac{r}{r_1}, \quad (62)$$

Here, r_0 and r_1 are positive constants. When $r \rightarrow +\infty$, we find

$$e^{2\nu} = e^{-2\lambda} = 1 - \frac{2M}{r} + \mathcal{O}(r^{-2}). \quad (63)$$

Therefore, the wormhole behaves as a positive mass object. On the other hand, when $r \rightarrow -\infty$, we find

$$e^{2\nu} = e^{-2\lambda} = 1 + \frac{2M}{|r|} + \mathcal{O}(r^{-2}). \quad (64)$$

Therefore, the wormhole behaves as an NMO.

We may consider the following time dependence,

$$\nu = -\lambda = -\frac{M \left(1 + \tanh \frac{t}{t_0}\right)}{\sqrt{r^2 + r_0^2}} \tanh \frac{r}{r_1}, \quad a = \frac{a_0}{2} \left(1 + \tanh \frac{t}{t_0}\right). \quad (65)$$

Here t_0 and a_0 are positive constants. When $t \rightarrow +\infty$, the spacetime corresponding to (65) goes to the wormhole spacetime in (61) with (62) and $a = a_0$. On the other hand, when $t \rightarrow -\infty$, the spacetime corresponding to (65) reduces to the flat spacetime,

$$ds^2 = dt^2 + dr^2 + r^2 (d\vartheta^2 + \sin^2 \vartheta d\varphi^2). \quad (66)$$

Therefore, the spacetime corresponding to (65) describes the creation of the wormhole. An interesting point is that there is a flow of mass from the universe corresponding to the negative r to the universe corresponding to the positive r . As a result, the positive mass object is created in the universe corresponding to the positive r , although an NMO is created in the universe corresponding to the negative r .

The above time-dependent geometry (61) with (65) by using the four scalar non-linear σ model in (49) with (50), (51) and (52) by the choice of (60).

The obtained wormhole (61) with (65) plays the role of a pump of matter, again. That is, the usual matter with positive mass may fall into the wormhole in our universe, but the fallen matter is blown out by the repulsive force due to the negative mass of the wormhole in another universe. For the electromagnetic wave or gravitational wave, there could occur the redshift or blueshift, again. Because the wormhole is dynamical, the effects of the pump, the redshift or the blueshift increase in time.

As in [59], we may consider the spacetime where the static wormhole geometry is expanding by a scale factor $e^{N(t)}$. We consider the following metric,

$$ds^2 = e^{2N(t)} \left\{ e^{2\nu(r)} dt^2 + e^{2\lambda(r)} dr^2 + (r^2 + r_0^2) (d\vartheta^2 + \sin^2 \vartheta d\varphi^2) \right\}, \quad \nu = -\lambda = -\frac{2M}{\sqrt{r^2 + r_0^2}} \tanh \frac{r}{r_1}. \quad (67)$$

Here r_0 is a constant. We may define the cosmological time τ by

$$d\tau \equiv e^{N(t)} dt. \quad (68)$$

When r is large, from the coefficient of $(d\vartheta^2 + \sin^2 \vartheta d\varphi^2)$, we may identify the radial coordinate ρ by

$$\rho \sim e^{N(t)} r. \quad (69)$$

Then as in (63) and (64), when $|r|$ is large, $e^{2\nu(r)}$

$$e^{2\nu(r)} \rightarrow 1 \mp \frac{2M}{r} \sim 1 \mp \frac{2Me^{N(t)}}{\rho}. \quad (70)$$

Therefore, the ADM mass is given by $\pm Me^{N(t)}$. If the universe is expanding, the (positive or negative) ADM mass grows, and the role of the pump becomes stronger and stronger. We should also note that the throat radius is given by $r_0 e^{N(t)}$, which also becomes larger when the universe is expanding. Due to the expansion of the universe, the wormhole could become traversable.

VII. PHOTON'S ORBITS

The lensing effects could observe the NMOs [19–25]. In this section, we review the lensing based on the previous paper, [41].

Since the ADM mass is negative in the spacetime of NMOs, the anti-gravity could work as a gravitational concave lens. In this section, we investigate the photon's orbit in the NMO geometry and the effects of lensing by assuming that the orbit can be given by a null orbit in a static, spherically symmetric spacetime.

The following Lagrangian describes the motion of the photon,

$$\mathcal{L} = \frac{1}{2} g_{\mu\nu} \dot{q}^\mu \dot{q}^\nu = \frac{1}{2} \left(-e^{2\nu} \dot{t}^2 + e^{2\lambda} \dot{r}^2 + r^2 \dot{\theta}^2 + r^2 \sin^2 \theta \dot{\varphi}^2 \right). \quad (71)$$

Here, the dot “ $\dot{}$ ” expresses the derivative with respect to the affine parameter. Because the Lagrangian \mathcal{L} does not depend on the t and φ , there exist conserved quantities corresponding to energy E and angular momentum L ,

$$E \equiv \frac{\partial \mathcal{L}}{\partial \dot{t}} = -e^{2\nu} \dot{t}, \quad (72)$$

$$L \equiv \frac{\partial \mathcal{L}}{\partial \dot{\varphi}} = r^2 \sin^2 \theta \dot{\varphi}. \quad (73)$$

The total energy \mathcal{E} of the system should be also conserved,

$$\mathcal{E} \equiv \mathcal{L} - \dot{t} \frac{\partial \mathcal{L}}{\partial \dot{t}} - \dot{r} \frac{\partial \mathcal{L}}{\partial \dot{r}} - \dot{\theta} \frac{\partial \mathcal{L}}{\partial \dot{\theta}} - \dot{\varphi} \frac{\partial \mathcal{L}}{\partial \dot{\varphi}} = \mathcal{L}. \quad (74)$$

In the case of a photon, whose geodesic is null, we require $\mathcal{E} = \mathcal{L} = 0$.

Without loss of generality, we consider the orbit on the equatorial plane with $\theta = \frac{\pi}{2}$. Then the condition $\mathcal{E} = \mathcal{L} = 0$ gives,

$$0 = -\frac{E^2}{2} + \frac{1}{2} \dot{r}^2 + \frac{L^2 a(r)}{2r^2}. \quad (75)$$

For simplicity, we considered the case of the Schwarzschild-type metric

$$e^{2\nu(r)} = e^{-2\lambda(r)} = 1 - \frac{2M}{r}. \quad (76)$$

If M is negative, the spacetime is given by an NMO.

This system is analogous to the classical dynamical system with potential $U(r)$,

$$0 = \frac{1}{2} \dot{r}^2 + U(r), \quad U(r) \equiv \frac{L^2 e^{2\nu(r)}}{2r^2} - \frac{E^2}{2}. \quad (77)$$

If there is a circular orbit, where $\dot{r} = 0$, the equations $U(r) = U'(r) = 0$ must have a solution. We find, however,

$$U(r) = \frac{L^2}{2r^2} \left(1 - \frac{2M}{r} \right) - \frac{E^2}{2}, \quad (78)$$

$$U'(r) = -\frac{L^2}{r} \left(\frac{1}{r^2} - \frac{3M}{r^3} \right), \quad (79)$$

Eq. (79) has no solution if M is negative, and therefore there is no circular orbit of a photon, nor a photon sphere when $M < 0$.

For Eq. (77) with (78), the radius of the turning point, where $\dot{r} = 0$ is given by

$$0 = U(r) = \frac{L^2}{2r^2} \left(1 - \frac{2M}{r} \right) - \frac{E^2}{2}. \quad (80)$$

which is a cubic algebraic equation, which can be solved.

$$r = \left(-q + \sqrt{\Delta} \right)^{\frac{1}{3}} + \left(-q - \sqrt{\Delta} \right)^{\frac{1}{3}}, \quad q \equiv \frac{L^2 M}{E^2}, \quad \Delta = \frac{L^4 M^2}{E^4} - \frac{L^6}{27E^6}. \quad (81)$$

Here we choose a real branch for $(\)^{\frac{1}{3}}$ although there are two complex branches besides the real one. Because $q^2 > \Delta$ and $-q > 0$, as long as $\Delta \geq 0$, Eq. (81) is a unique and positive solution of r . Even if $\Delta < 0$, because the second term in Eq. (81) is the complex conjugate of the first term, Eq. (81) gives a real and positive solution for r . We should note that because Eq. (79) tells that $U'(r) < 0$, that is, $U(r)$ is a monotonically decreasing function of r as long as $r > 0$, Eq. (80) has a unique real and positive solution of r , which is the minimum radius or the turning point of the orbit.

As in classical mechanics, the solution of (77) is given by

$$t = \int \frac{dr}{\sqrt{-2U(r)}} = \int \frac{dr}{\sqrt{E^2 - \frac{L^2}{r^2} \left(1 - \frac{2M}{r} \right)}}, \quad (82)$$

or because Eq. (73) with $\theta = \frac{\pi}{2}$ tells $\frac{d\varphi}{dt} = \frac{L}{r^2}$, we rewrite (77) with (78) in the following form,

$$0 = \frac{L^2}{2r^4} \left(\frac{dr}{d\varphi} \right)^2 + \frac{L^2}{2r^2} \left(1 - \frac{2M}{r} \right) - \frac{E^2}{2}, \quad (83)$$

which can be integrated to give,

$$\varphi = \int \frac{dr}{r^2 \sqrt{\frac{E^2}{L^2} - \frac{1}{r^2} \left(1 - \frac{2M}{r} \right)}}, \quad (84)$$

which gives the shape of the orbit. An asymptotically hyperbolic curve could give the orbit for NMOs, where M is negative. Therefore, the NMO can be regarded as a gravitational concave lens. If the NMO exists in front of the light source(s), for example, a small NMO in front of the sun, the object could be observed as a dark spot. If there are many light sources behind the NMO, we can observe the deformed distribution as observed in [19–25].

VIII. RAY-TRACING AND SHADOWS

Let us now analyse the optical appearance of such a type of wormhole. To do so, we use the so-called ray-tracing technique that integrates the photon trajectory from the observer screen towards the object. The motion is just described by the geodesic equation (75), which can be rewritten in the form:

$$\dot{r}^2 = \frac{1}{b^2} - V(r), \quad (85)$$

where the parameter b is the so-called impact parameter $b = \frac{L}{E} = \frac{g_{\theta\theta}\dot{\phi}}{g_{tt}\dot{t}}$ and it describes each photon trajectory, whereas the effective potential is given by:

$$V(r) = \frac{g_{tt}}{g_{\theta\theta}}. \quad (86)$$

Here, g_{tt} and $g_{\theta\theta}$ stand for the corresponding components of the metric, which are assumed to be static and spherically symmetric. The shape of the potential is shown in Fig. 4, where one can note the asymmetry between both sides of the throat for the wormhole (43). Also, the effective potential for the Schwarzschild black hole is depicted, which shows a pole at the origin as expected due to the presence of a singularity. We have also included the Simpson-Visser wormhole, whose metric can be expressed as follows [62],

$$ds^2 = - \left(1 - \frac{2M}{\sqrt{r^2 + a^2}} \right) dt^2 + \left(1 - \frac{2M}{\sqrt{r^2 + a^2}} \right)^{-1} dr^2 + (r^2 + a^2) d\Omega^2. \quad (87)$$

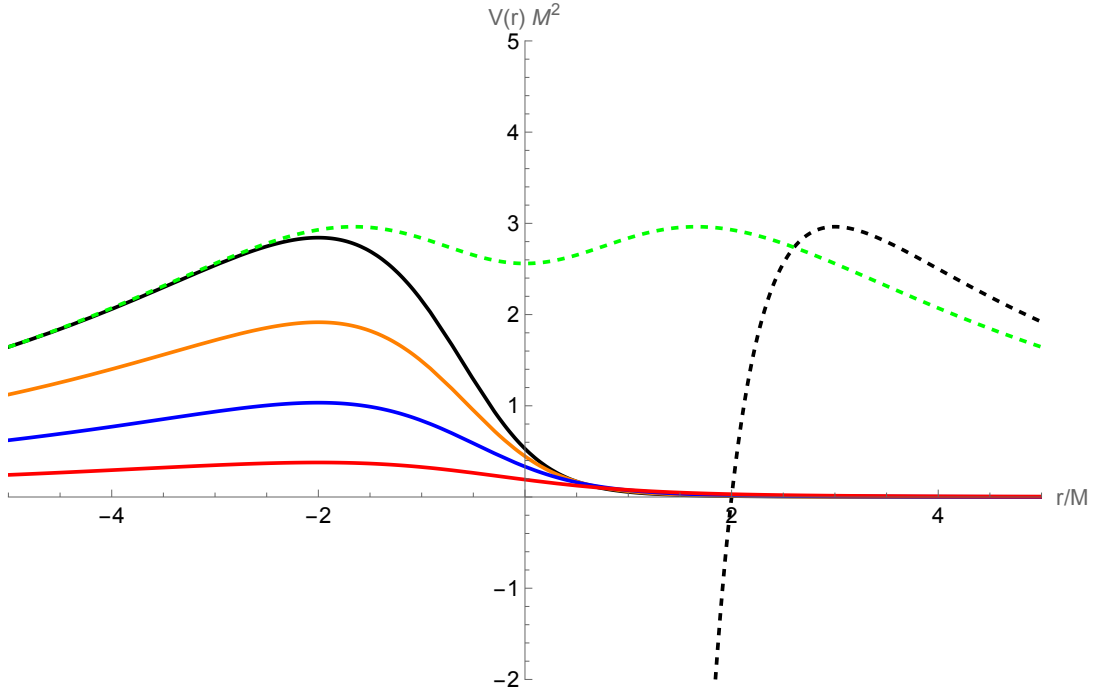


FIG. 4. The effective potential for photons (86). The curves describe the Schwarzschild case (dashed black line), the Simpson-Visser wormhole with $a/M = 5/2$ (dashed green line) and the wormhole (43) for $q/M = 1.7$ (black), $q/M = 1.8$ (orange), $q/M = 2$ (blue), $q/M = 2.5$ (red). Note that to visualise all the potentials better, the scales of the Schwarzschild black hole and for the Simpson-Visser wormhole are increased by a factor $\times 80$.

One should also note that the wormhole potential exhibits an unstable circular orbit for photons just in one of the sides of the throat, while it does not at the other side. The equation of the trajectory in the equatorial plane (84) can be expressed as:

$$\left(\frac{d\phi}{dr}\right) = \pm \frac{b}{g_{\theta\theta} \sqrt{1 - \frac{b^2 g_{tt}}{g_{\theta\theta}}}}, \quad (88)$$

In Fig. 5, a set of trajectories is simulated for a particular range of the impact parameter. Then, the aim is to use where photons cross a hypothetical accretion disk around the wormhole in order to simulate the observed luminosity. By assuming the accretion disk to be located perpendicular to the line of sight of the observer, which in Fig. 5 would refer to the vertical axes, we can compute the observed luminosity. To do so, one should note that for some values of the impact parameter, photon trajectories cross the vertical axes, and consequently the accretion disk, more than once, which implies an additional brightness in the observer screen due to the extra photons approaching with the same impact parameter but emitted at different locations of the accretion disk. To compute the total luminosity, one has to sum over all the contributions:

$$I_{\text{obs}} = \sum_m g_{tt}(r)^2 I^{\text{em}}(r) \Big|_{r=r_m(b)}, \quad (89)$$

where $I(r)$ is the luminosity profile of the accretion disk and $r_m(b)$ are the so-called transfer functions that characterise the location of photon emission as a function of the impact parameter. Such transfer functions are depicted in Fig. 6, where the subscript m refers to the direct emission ($m = 0$), the lensed emission ($m = 1$) and higher order emissions ($m \geq 2$), which just collect the locations where a photon with a particular impact parameter might intersect the central object according to its trajectory. Moreover, for describing the emission of the accretion disk, we are assuming a particular intensity profile that, despite its simplicity, might describe the emission of the accretion disk effectively according to previous gravitomagnetic-hydrodynamics simulations [63]. Such a profile can be cast as follows:

$$I^{\text{em}}(r, \tilde{\mu}, \sigma, \gamma) = \frac{e^{-\frac{1}{2}[\gamma + \text{arcsinh}(\frac{r-\tilde{\mu}}{\sigma})]^2}}{\sqrt{(r - \tilde{\mu})^2 + \sigma^2}}. \quad (90)$$

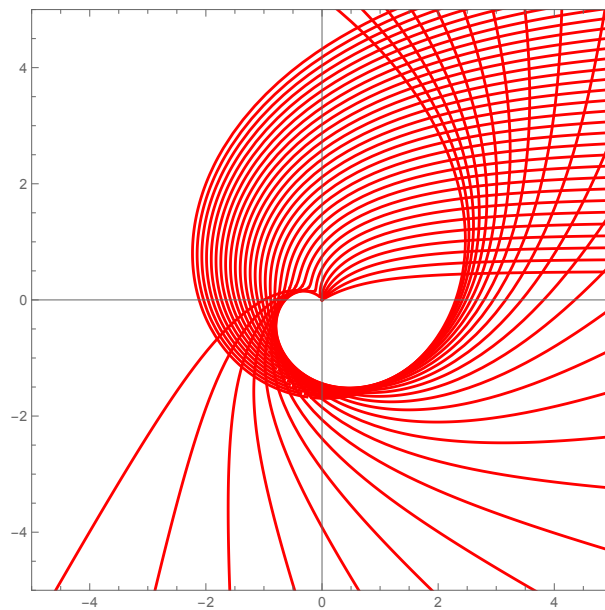


FIG. 5. Light trajectories in the equatorial plane for the wormhole (43) with $q/M = 1.8$ and an interval of the impact parameter $b \in (0, 10)$.

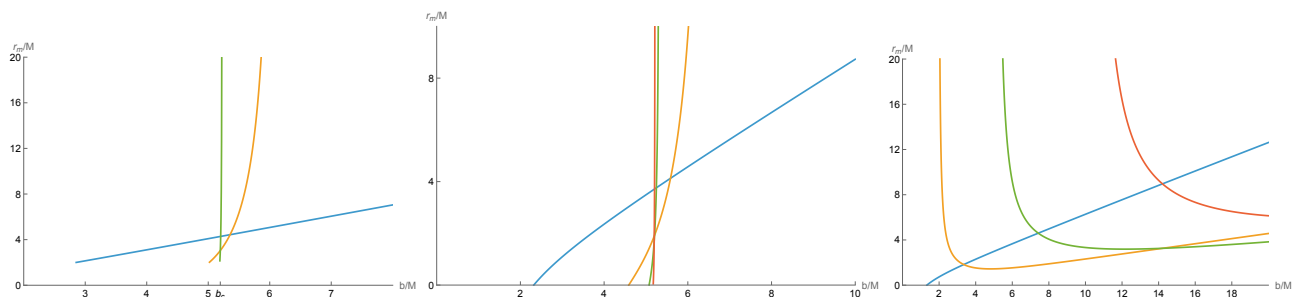


FIG. 6. Transfer functions for the Schwarzschild black hole (left panel), the Simpson-Visser wormhole with $a/M = 5/2$ (central panel) and the wormhole (43) with $q/M = 1.8$ (right panel). The plots show the curves for the direct emission (blue), the lensed emission (orange) and higher order cases (green and red).

Here, $\tilde{\mu}$, σ and γ are free parameters that describe the position of the emission peak, its width and the size of the central region, respectively. Fig. 7 gives a representation of such a type of profile. For the sake of this work, we are considering for every simulation the same width and size for the intensity but varying the location of the peak, as shown in Fig. 7. Note also that for the case of the NMO wormhole (43), the intensity profile is assumed to have its peak at the throat $r = 0$, at the location of the ISCO $r = 0.49$, but also at $r = 3M$ and at $r = 6M$, where the photon sphere and the ISCO are located for the Schwarzschild black hole. This is because the wormhole (43) has no circular orbit for photons for $r > 0$, as it is inferred in the shape of the potential in Fig. 4, while ISCO is very close to the central object $r/M = 0.49$, so that in order to guarantee a better comparison, we also include such simulations.

Then, in Figs. 8, 9 and 10, the luminosity as collected by a far away observer is depicted for the Schwarzschild black hole, the Simpson-Visser wormhole [62] and the wormhole (43) with $q/M = 1.8$. As such figures point out, the photon rings' substructure is much more complex in the case of the NMO wormhole when the peak of the luminosity is a bit far away from the throat, not only in comparison to the Schwarzschild black hole but also when comparing to another wormhole structure. Such a result is a direct consequence of the asymmetry of the effective potential 4 in the NMO wormhole, which exhibits a maximum (a circular orbit for photons) on the other side of the throat, which affects what an observer would collect on the screen at the positive side of the throat. Nevertheless, when the peak of the luminosity is close to the throat, and particularly to the ISCO, differences are not so notorious despite the observed luminosity reaching the throat in comparison to the Simpson-Visser wormhole, where it does not.

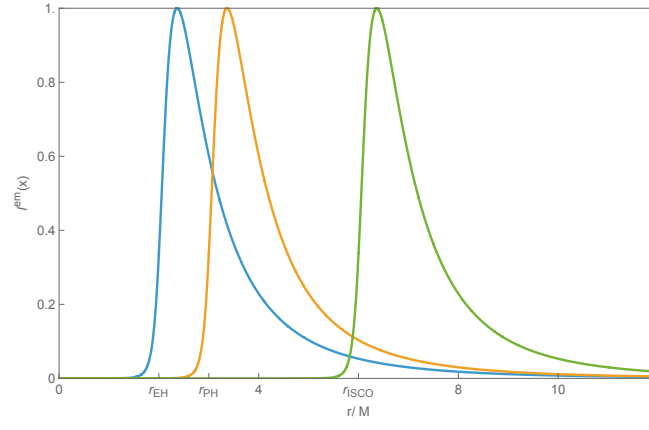


FIG. 7. The intensity profile (90) with $\gamma = -2$, $\sigma = 1/4$ and $\tilde{\mu} = 2$ (blue), $\tilde{\mu} = 3$ (orange) and $\tilde{\mu} = 6$ (green), which refer to the location of the event horizon, the photon sphere and the ISCO for a Schwarzschild black hole.

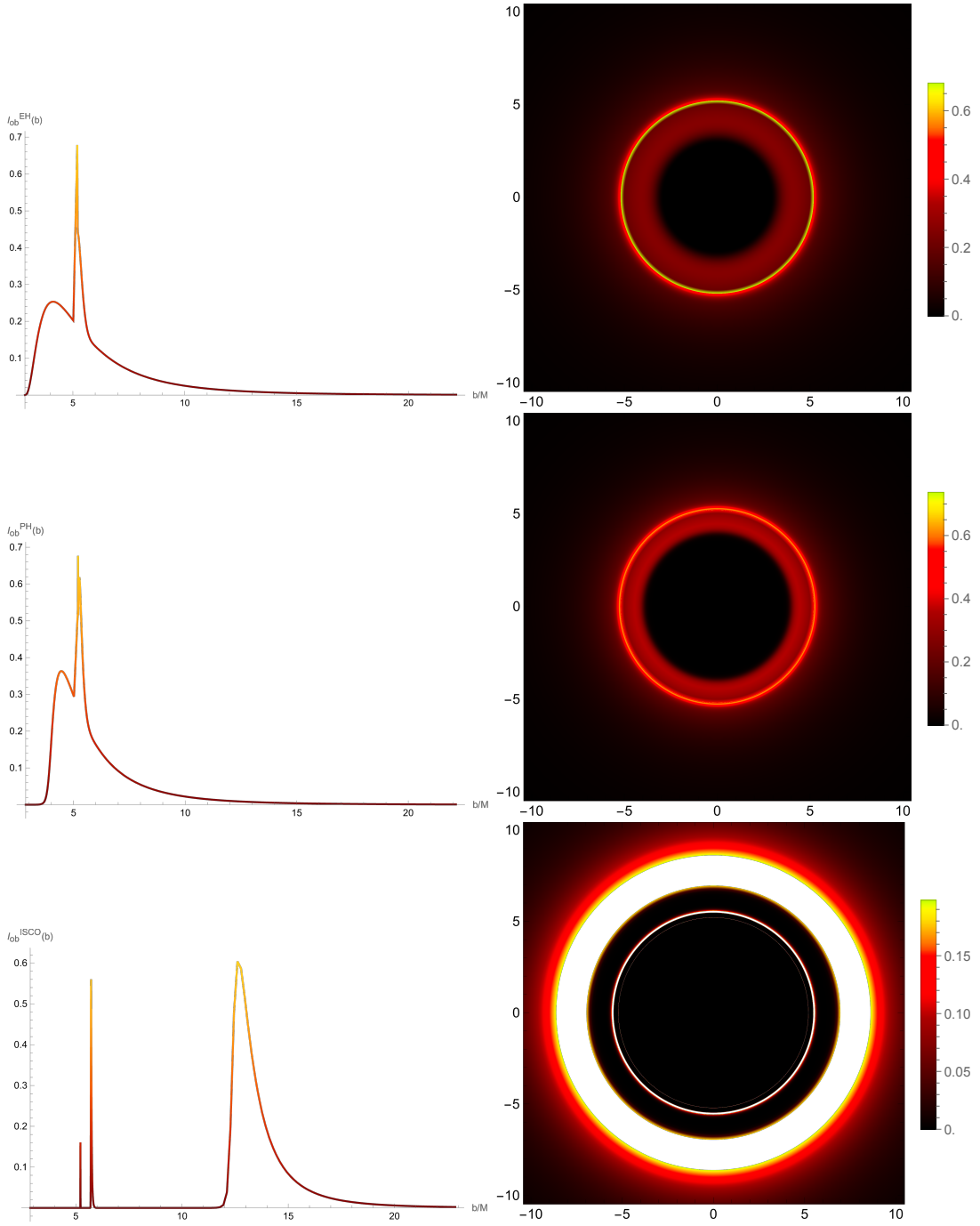


FIG. 8. Observed intensities (left panels) and the shadows (right panels) for a Schwarzschild black hole. From top to the bottom: the peak of the luminosity located at $r = 2M$ (Event horizon), at $r = 3M$ (photon sphere) and at $r = 6M$ (ISCO).

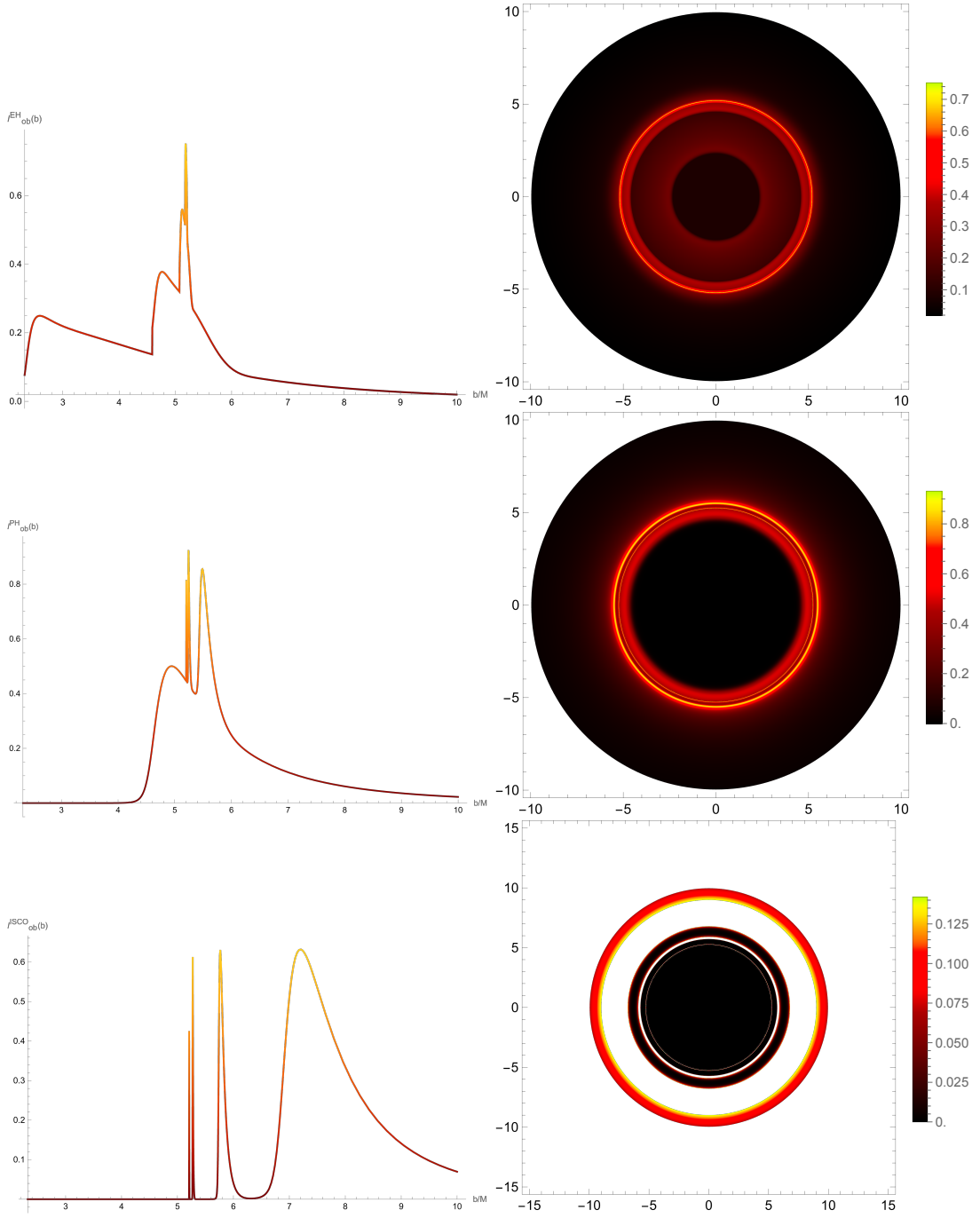


FIG. 9. Observed intensities (left panels) and the shadows (right panels) for a Simpson-Visser wormhole with $a = 5/2$. From top to the bottom: the peak of the luminosity located at $r = 0$ (the throat), at $r = 3M$ (photon sphere) and at $r = 5.45M$ (ISCO).

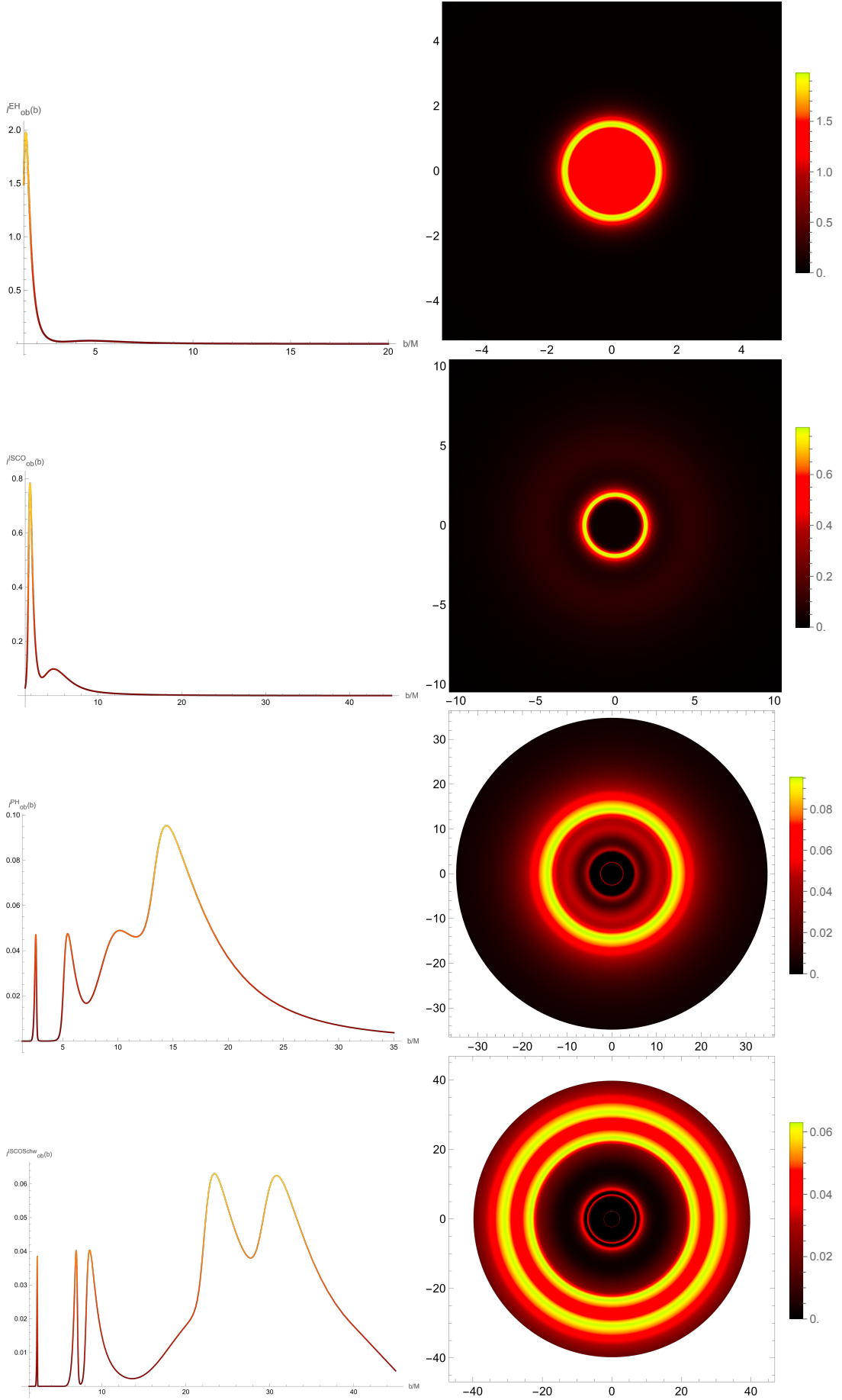


FIG. 10. Observed intensities (left panels) and the shadows (right panels) for the wormhole black hole (43) with $q/M = 1.8$. From top to the bottom, the locations of the peaks are at $r = 0$ (the throat), $r = 0.49M$ (ISCO), $r = 3M$ (Schwarzschild photon sphere) and $r = 6M$ (Schwarzschild ISCO).

IX. SUMMARY AND DISCUSSION

In this paper, we have investigated systems containing NMOs. By starting with a tutorial review of the classical mechanics of a system including NMOs in Section II, we have found that a system consisting of one object with positive mass and one NMO, a bound state exists even though the force exerted by the NMO on the object with positive mass is repulsive. Unlike a standard system consisting of two objects with positive mass, the gravitational waves emitted from this system exhibit a decrease in frequency and amplitude over time, as shown in Section III. In Section IV, we propose a formulation to exclude the ghosts that arise in the model realising the Ellis-Bronnikov wormhole [16, 17], a candidate of an NMO. We also construct a model of the time evolution of the Ellis-Bronnikov wormhole in Section VI, by using the non-linear σ model reviewed in Section V.

After reviewing the lensing effect by the NMOs in Section VII, by using the so-called ray-tracing technique, we have shown the numerical results for the observed image of NMOs or the Ellis-Bronnikov wormhole, numerically in Section VIII. By computing the luminosity and optical appearance of the NMO wormhole in comparison to the canonical Schwarzschild black hole and the Simpson-Visser wormhole, large differences arise in the intensity and the images as a result of the asymmetric potential for the photons' trajectories that characterises such NMO objects, showing a much more complex photon rings substructure in some cases. One should note that the asymmetry potential for photon trajectories depicted in Fig. 4 shows that on one side of the throat ($r < 0$) it has a similar shape as other more usual objects, such as the Simpson-Visser spacetime and even, up to some limit, to the Schwarzschild black hole. This means that for $r < 0$, photons will follow similar paths as in Simpson-Visser spacetime. Indeed, differences arise when dealing with the other side of the throat ($r > 0$), where the absence of a maximum in the photon's potential avoids possible locations for any circular photon orbits. In addition, the potential remains constant and small till one approaches the central object closely, which produces a high deflection on the photons that are emitted by the accretion disk far from the central object, while its luminosity decreases very fast when the peak is close to the throat. The result in the optical appearance of the object is an interesting structure of photon rings surrounding the object that shows large differences with other spacetimes. Firstly, when the peak of the luminosity is located at the wormhole throat, the observed intensity also reaches the throat, contrary to the Simpson-Visser wormhole [47]. Moreover, when the peak is located further from the throat, one finds that those photons experience high deflections, leading to an observed luminosity that contains several peaks that then give a complex photon ring structure in comparison to the other two spacetimes.

Although one might not expect the existence of such objects, this analysis intends to give a smoking gun that might be used in the future to infer the existence of objects beyond the Kerr paradigm and the current fundamental physics.

ACKNOWLEDGEMENTS

DS-CG is supported by the Spanish project PID2024-157196NB-I00 funded by MICIU/AEI/10.13039/501100011033 (“ERDF A way of making Europe”, “PGC Generación de Conocimiento”); and the financial support by the Department of Education, Junta de Castilla y León and FEDER Funds, Ref. CLU-2023-1-05.

-
- [1] J. M. Luttinger, Gravity Research Foundation, <https://static1.squarespace.com/static/5852e579be659442a01f27b8/t/5873dc04d1758eea4b41c720/1483987972731/luttinger.pdf> (1951).
 - [2] H. Bondi, *Rev. Mod. Phys.* **29**, 423 (1957).
 - [3] J. S. Farnes, *Astron. Astrophys.* **620**, A92 (2018), arXiv:1712.07962 [physics.gen-ph].
 - [4] J. Belletère and M. B. Paranjape, *Int. J. Mod. Phys. D* **22**, 1341017 (2013), arXiv:1304.1566 [gr-qc].
 - [5] W. B. Bonnor, *Gen Relat Gravit* **21**, 1143 (1989).
 - [6] H. Cebeci, O. Sarioglu, and B. Tekin, *Phys. Rev. D* **73**, 064020 (2006), arXiv:hep-th/0602117.
 - [7] R. B. Mann, *Class. Quant. Grav.* **14**, 2927 (1997), arXiv:gr-qc/9705007.
 - [8] R. L. Forward, *Journal of Propulsion and Power* **6**, 28 (1990).
 - [9] C. B. Møller, R. A. Thomas, G. Vasilakis, E. Zeuthen, Y. Tsaturyan, M. Balabas, K. Jensen, A. Schliesser, K. Hammerer, and E. S. Polzik, *Nature* **547**, 191 (2017), arXiv:1608.03613 [quant-ph].
 - [10] M. A. Khamehchi, K. Hossain, M. E. Mossman, Y. Zhang, T. Busch, M. M. Forbes, and P. Engels, *Phys. Rev. Lett.* **118**, 155301 (2017).
 - [11] H. Socas-Navarro, *Astron. Astrophys.* **626**, A5 (2019), arXiv:1902.08287 [astro-ph.CO].
 - [12] J. P. Petit and G. d’Agostini, *Astrophys. Space Sci.* **354**, 2106 (2014).

- [13] S. Nájera, A. Gamboa, A. Aguilar-Nieto, and C. Escamilla-Rivera, *Astron. Astrophys.* **651**, L13 (2021), arXiv:2105.11041 [gr-qc].
- [14] G. Manfredi, J.-L. Rouet, B. Miller, and G. Chardin, *Phys. Rev. D* **98**, 023514 (2018), arXiv:1804.03067 [gr-qc].
- [15] O. Trivedi and A. Loeb, (2026), arXiv:2605.10976 [gr-qc].
- [16] H. G. Ellis, *J. Math. Phys.* **14**, 104 (1973).
- [17] K. A. Bronnikov, *Acta Phys. Polon. B* **4**, 251 (1973).
- [18] H. Huang, H. Lü, and J. Yang, *Class. Quant. Grav.* **39**, 185009 (2022), arXiv:2010.00197 [gr-qc].
- [19] J. G. Cramer, R. L. Forward, M. S. Morris, M. Visser, G. Benford, and G. A. Landis, *Phys. Rev. D* **51**, 3117 (1995), arXiv:astro-ph/9409051.
- [20] M. Safonova, D. F. Torres, and G. E. Romero, *Mod. Phys. Lett. A* **16**, 153 (2001), arXiv:astro-ph/0104075.
- [21] M. Safonova, D. F. Torres, and G. E. Romero, *Phys. Rev. D* **65**, 023001 (2002), arXiv:gr-qc/0105070.
- [22] E. Eiroa, G. E. Romero, and D. F. Torres, *Mod. Phys. Lett. A* **16**, 973 (2001), arXiv:gr-qc/0104076.
- [23] M. Safonova and D. F. Torres, *Mod. Phys. Lett. A* **17**, 1685 (2002), arXiv:gr-qc/0208039.
- [24] R. Shaikh and S. Kar, *Phys. Rev. D* **96**, 044037 (2017), arXiv:1705.11008 [gr-qc].
- [25] R. Takahashi and H. Asada, *Astrophys. J. Lett.* **768**, L16 (2013), arXiv:1303.1301 [astro-ph.CO].
- [26] L. Chetouani and G. Clément, *Gen. Rel. Grav.* **16**, 111 (1984).
- [27] V. Perlick, *Phys. Rev. D* **69**, 064017 (2004), arXiv:gr-qc/0307072.
- [28] F. Abe, *Astrophys. J.* **725**, 787 (2010), arXiv:1009.6084 [astro-ph.CO].
- [29] K. Nakajima and H. Asada, *Phys. Rev. D* **85**, 107501 (2012), arXiv:1204.3710 [gr-qc].
- [30] Y. Toki, T. Kitamura, H. Asada, and F. Abe, *Astrophys. J.* **740**, 121 (2011), arXiv:1107.5374 [astro-ph.CO].
- [31] N. Tsukamoto, T. Harada, and K. Yajima, *Phys. Rev. D* **86**, 104062 (2012), arXiv:1207.0047 [gr-qc].
- [32] N. Tsukamoto, M. Kimura, and T. Harada, *Phys. Rev. D* **89**, 024020 (2014), arXiv:1310.5716 [gr-qc].
- [33] C.-M. Yoo, T. Harada, and N. Tsukamoto, *Phys. Rev. D* **87**, 084045 (2013), arXiv:1302.7170 [gr-qc].
- [34] K. Izumi, C. Hagiwara, K. Nakajima, T. Kitamura, and H. Asada, *Phys. Rev. D* **88**, 024049 (2013), arXiv:1305.5037 [gr-qc].
- [35] K. Nakajima, K. Izumi, and H. Asada, *Phys. Rev. D* **90**, 084026 (2014), arXiv:1404.2720 [gr-qc].
- [36] V. Bozza and A. Postiglione, *JCAP* **06**, 036 (2015), arXiv:1502.05178 [gr-qc].
- [37] V. Bozza and C. Melchiorre, *JCAP* **03**, 040 (2016), arXiv:1511.07991 [gr-qc].
- [38] N. Tsukamoto and Y. Gong, *Phys. Rev. D* **97**, 084051 (2018), arXiv:1711.04560 [gr-qc].
- [39] V. Bozza, *Int. J. Mod. Phys. D* **26**, 1741013 (2017).
- [40] H. Asada, *Mod. Phys. Lett. A* **32**, 1730031 (2017), arXiv:1711.01730 [gr-qc].
- [41] S. Nojiri and S. D. Odintsov, (2026), arXiv:2602.15058 [gr-qc].
- [42] K. Akiyama *et al.* (Event Horizon Telescope), *Astrophys. J. Lett.* **875**, L1 (2019), arXiv:1906.11238 [astro-ph.GA].
- [43] K. Akiyama *et al.* (Event Horizon Telescope), *Astrophys. J. Lett.* **930**, L12 (2022), arXiv:2311.08680 [astro-ph.HE].
- [44] C.-K. Chan, D. Psaltis, F. Özel, R. Narayan, and A. Skadowski, *Astrophys. J.* **799**, 1 (2015), [Erratum: *Astrophys. J.* 807, 114 (2015)], arXiv:1410.3492 [astro-ph.HE].
- [45] S. E. Gralla, D. E. Holz, and R. M. Wald, *Phys. Rev. D* **100**, 024018 (2019), arXiv:1906.00873 [astro-ph.HE].
- [46] V. Perlick and O. Y. Tsupko, *Phys. Rept.* **947**, 1 (2022), arXiv:2105.07101 [gr-qc].
- [47] M. Guerrero, G. J. Olmo, D. Rubiera-Garcia, and D. S.-C. Gómez, *JCAP* **08**, 036 (2021), arXiv:2105.15073 [gr-qc].
- [48] Z. Younsi, D. Psaltis, and F. Özel, *Astrophys. J.* **942**, 47 (2023), arXiv:2111.01752 [astro-ph.HE].
- [49] S. Vagnozzi *et al.*, *Class. Quant. Grav.* **40**, 165007 (2023), arXiv:2205.07787 [gr-qc].
- [50] G. J. Olmo, D. Rubiera-Garcia, and D. S.-C. Gómez, *Phys. Lett. B* **829**, 137045 (2022), arXiv:2110.10002 [gr-qc].
- [51] G. J. Olmo, J. L. Rosa, D. Rubiera-Garcia, A. Rueda, and D. Sáez-Chillón Gómez, *Phys. Rev. D* **112**, 084059 (2025), arXiv:2507.16580 [gr-qc].
- [52] G. Manfredi, J.-L. Rouet, and B. Miller, (2026), arXiv:2601.22910 [astro-ph.CO].
- [53] S. Nojiri and S. D. Odintsov, *Phys. Lett. B* **779**, 425 (2018), arXiv:1711.00492 [astro-ph.CO].
- [54] S. Nojiri, S. D. Odintsov, and V. Folomeev, *Phys. Rev. D* **109**, 104007 (2024), arXiv:2401.15868 [gr-qc].
- [55] S. Nojiri and G. G. L. Nashed, *Phys. Rev. D* **108**, 124049 (2023), arXiv:2309.12379 [hep-th].
- [56] S. Nojiri and G. G. L. Nashed, *JCAP* **03**, 023 (2024), arXiv:2310.16068 [gr-qc].
- [57] E. Elizalde, S. Nojiri, S. D. Odintsov, and V. K. Oikonomou, *Phys. Dark Univ.* **45**, 101536 (2024), arXiv:2312.02889 [gr-qc].
- [58] S. Nojiri, S. D. Odintsov, and A. Sedrakian, *Nucl. Phys. B* **1006**, 116628 (2024), arXiv:2312.15839 [gr-qc].
- [59] T. Katuragawa, S. Nojiri, and S. D. Odintsov, *Phys. Dark Univ.* **51**, 102213 (2026), arXiv:2511.03275 [gr-qc].
- [60] G. G. L. Nashed and S. Nojiri, *Phys. Dark Univ.* **46**, 101655 (2024), arXiv:2402.12860 [gr-qc].
- [61] T. Katuragawa, S. Nojiri, and S. D. Odintsov, *Phys. Rev. D* **110**, 064014 (2024), arXiv:2406.18368 [gr-qc].
- [62] A. Simpson and M. Visser, *JCAP* **02**, 042 (2019), arXiv:1812.07114 [gr-qc].
- [63] H. Pagnat, A. Lupsasca, F. Vincent, and M. Wielgus, *Astron. Astrophys.* **668**, A11 (2022), arXiv:2206.02781 [astro-ph.HE].